Real roles of perylenetetracarboxylic diimide for enhancing photocatalytic H₂-production

Ting Sun [a], Jingang Song [a], Jiong Jia [a], Xiyou Li [a,b,*], Xuan Sun [a,*]

[a] Key Laboratory of Colloid and Interface Chemistry, Ministry of Education, School of Chemistry and Chemical Engineering, Shandong University, Jinan 250100, PR China
[b] College of Science, China University of Petroleum, Qingdao 266580, PR China

ARTICLE INFO

ABSTRACT

On account of the steps of water splitting reaction, suppression of the electron–hole recombination is one key factor to improve the photocatalytic activity. Composites with π-conjugated molecules are promising to inhibit the recombination process by delocalization of the photo-generated electron. In this study, we synthesized perylenetetracarboxylic diimide (**PDI**) decorated $Zn_{0.5}Cd_{0.5}S$ hybrid photocatalysts to reveal the function of the **PDI** in promoting the charge separation by electron transfer process. To understand the mechanisms that govern the carrier separation, transport, extraction and their recombination within this inorganic/organic nanocomposite, three **PDIs**, namely **PDI-1**, **PDI-2** and **PDI-3** with different molecular structure were loaded in the $Zn_{0.5}Cd_{0.5}S$, respectively, and were investigated comparatively. It is demonstrated that **PDIs** play great roles in increasing the specific surface area and stabilizing the photogenerated electron–hole pairs, resulting in enhancement of the overall hydrogen production rate. The highest rate of 1.32 mmol h^{-1} g^{-1} was achieved on the $Zn_{0.5}Cd_{0.5}S$-**PDI-1** composite, which is 6 times higher than the pristine $Zn_{0.5}Cd_{0.5}S$, owning to the effective photo-driven electron transport between the $Zn_{0.5}Cd_{0.5}S$ and the **PDI-1**. The results of the current work are relevant in understanding the nature of charge-transfer pathways in photoinduced catalysis.

© 2016 Elsevier Ltd. All rights reserved.

1. Introduction

In response to the increasing concerns over issues of environmental protection and sustainable energy supply, hydrogen production from water splitting reaction using semiconductors (SCs) as photocatalysts has attracted broad attention as an effective route for solar energy conversion, which is clean, renewable and inexpensive. Since the first report on photoelectrochemical water splitting on a TiO₂ SC electrode by Fujishima and Honda [1], significant progress in this regard led to the development of photocatalysts applicable to a wide region of the solar spectrum. Metal sulfides and sulfide solid solutions have attracted great interest due to their suitable band gap for efficient utilization of visible light [2]. $Zn_xCd_{1-x}S$ solid solution has been fully proved to be an efficient, low-toxic, and cost-effective visible-light driven photocatalysts for H₂-evlution from water splitting [3–10]. However, further improvement of the photocatalytic efficiency was retarded by factors such as a high recombination rate of photogenerated electron−hole pairs. Many attempts have been tried to suppress

this recombination, including loading cocatalyst such as metal sulfides [11], metal oxides [12,13], and carbon nanotubes [14,15], to alternatively trap the photogenerated electrons or holes, or by doping with other metals to promote the charge separation and/or function as separated redox reaction sites [16,17].

Indeed, the efficient photocatalytic conversion of liquid water to hydrogen and oxygen gases has been proved by natural photosynthesis with organic dyes as light harvester and catalysts via a multi-electron process. This multi-electron transfer process should be of significant for preventing $e^-−h^+$ recombination and therefore the highly efficient photosynthesis. In view of this perspective, combination of the organic dyes with SCs catalysts to construct multistep electron transfer process may provide opportunities for stabilizing the charge carriers. Perylene tetracarboxylic diimide (**PDI**) derivatives are promising molecular building blocks for electron-transporting materials based on their robust nature of high thermal and oxidative stability in air and water. Specifically, **PDI** bares an electron-delocalized planar framework, which makes it highly electron-deficient n-type semiconductor with lower reduction potential and high electron affinities. The optical and electrochemical properties of **PDIs** can be fine-tuned by bay-position substitution [18–25], while imide nitrogen can be facilely

modified to adjust the packing and electronic coupling between neighbouring **PDIs** in solid state. As the visible-light collector, perylene derivatives have been investigated in photoelectrochemical water-splitting systems [26–28]. Quite recently, Caramori and Bignozzi et al. [29] used dicationic PDI as sensitizer to inject charges to WO_3, which resulted in long-lived charge separated states in the heterogeneous phase and hole transfer to the sacrificial hole scavenger for photo-oxidation reactions.

Herein, we study the organic-inorganic composites as photocatalysts for visible-light driven H_2 production. **PDIs** decorated **Zn$_{0.5}$Cd$_{0.5}$S** solid solutions were prepared with a facile in-situ synthetic method. Primarily, **PDIs** within the composites are proposed to be the electron acceptor, which played a crucial factor in suppressing the recombination of the photogenerated electrons and holes. Indeed, as demonstrated in previous work [30], electron-transfer occurred from **PDI** molecules to **CdS** in the **CdS–PDI** composites, resulting in synergetic semiconducting properties and therefore the significantly enhanced conductivity of the organic–inorganic hybrid. To get insight into the real functions of the **PDIs** and the electron-transporting mechanism within the hybrids, three **PDI** derivatives, [(N,N′-diethoxyperylene-3,4,9,10-tetra-carboxylic acid diimide)] (**PDI-1**), − 1,7-bis(p-t-butyl-phenoxyl) perylene (**PDI-2**), and -1,6,7,12-tetra(p-t-butyl-phenoxyl) perylene (**PDI-3**), with different numbers of p-t-butyl-phenoxyl groups at the bay-position as shown in Scheme 1, were blended with **Zn$_{0.5}$Cd$_{0.5}$S**, respectively. The photocatalytic activity was drastically improved after loading a very small amount of **PDIs** with the molar ratio of 0.5% (Fig. S1b). The dependence of the H_2-evolution rate on the loaded **PDIs** with different molecular structures suggests the key role of the **PDIs** in suppressing the charge recombination for enhancing photocatalytic H_2-production.

2. Results and discussion

2.1. Fabrication of Zn$_{0.5}$Cd$_{0.5}$S-PDIs hybrid material and microstructure characterization

The **Zn$_x$Cd$_{1−x}$S-PDIs** nanocomposites were fabricated by in-situ loading the **PDIs** onto the preformed **Zn$_x$Cd$_{1−x}$S** solid solutions. To enhance coupling the dyes with **Zn$_x$Cd$_{1−x}$S**, hydroxyl groups were introduced to the end position (imide nitrogen) of the **PDIs** (Scheme S1–S3, ESI†). Initially, **Zn$_x$Cd$_{1−x}$S** solid solutions (x=0.1, 0.3, 0.5, 0.7, 0.9) were prepared with diverse molar ratio of Zn^{2+}/Cd^{2+} according to a well-established procedure (ESI†). The highest H_2-evolution rate for the **Zn$_x$Cd$_{1−x}$S** was observed at x=0.5 (215 μmol $h^{−1}$ $g^{−1}$, Fig. S1 a) [7,17,31,32]. We therefore use the **Zn$_{0.5}$Cd$_{0.5}$S** solid solution in the following study. Specified mass of **PDI-1** were dispersed in DMF and added into the **Zn$_{0.5}$Cd$_{0.5}$S** solid solution with different **PDI-1/Zn$_{0.5}$Cd$_{0.5}$S** weight ratios (ESI†). Interestingly, the photocatalytic activity of **Zn$_{0.5}$Cd$_{0.5}$S/PDI-1** photocatalysts with different amounts of **PDI-1** in the nanocomposite improved drastically as shown in Fig. S1b. The highest initial H_2 evolution rate of 1.32 mmol $h^{−1}$ $g^{−1}$ was achieved when **PDI-1** loading ratio is 0.5% (vid infra), labelled as **Zn$_{0.5}$Cd$_{0.5}$S-PDI-1**, which was nearly 6 times of the naked **Zn$_{0.5}$Cd$_{0.5}$S**. Further increasing the **PDI-1** content in the hybrids led to a gradual reduction of the photocatalytic activity. To disclose the effects of **PDIs** on the photocatalytic activity, the other two **PDI** derivatives **PDI-2** and **PDI-3** with two or four butyl-phenoxyl groups at the bay-position were synthesized and well characterized (Schemes S2 and S3, ESI†), since the reduction potentials of **PDIs** depend heavily on the bay-substitution, which is beneficial for tuning the interactions between the **PDIs** and **Zn$_{0.5}$Cd$_{0.5}$S**. **PDI-2** and **PDI-3** with weight ratio of 0.5% were loaded into the **Zn$_{0.5}$Cd$_{0.5}$S** to form **Zn$_{0.5}$Cd$_{0.5}$S-PDI-2**, and **Zn$_{0.5}$Cd$_{0.5}$S-PDI-3** nanocomposite, respectively.
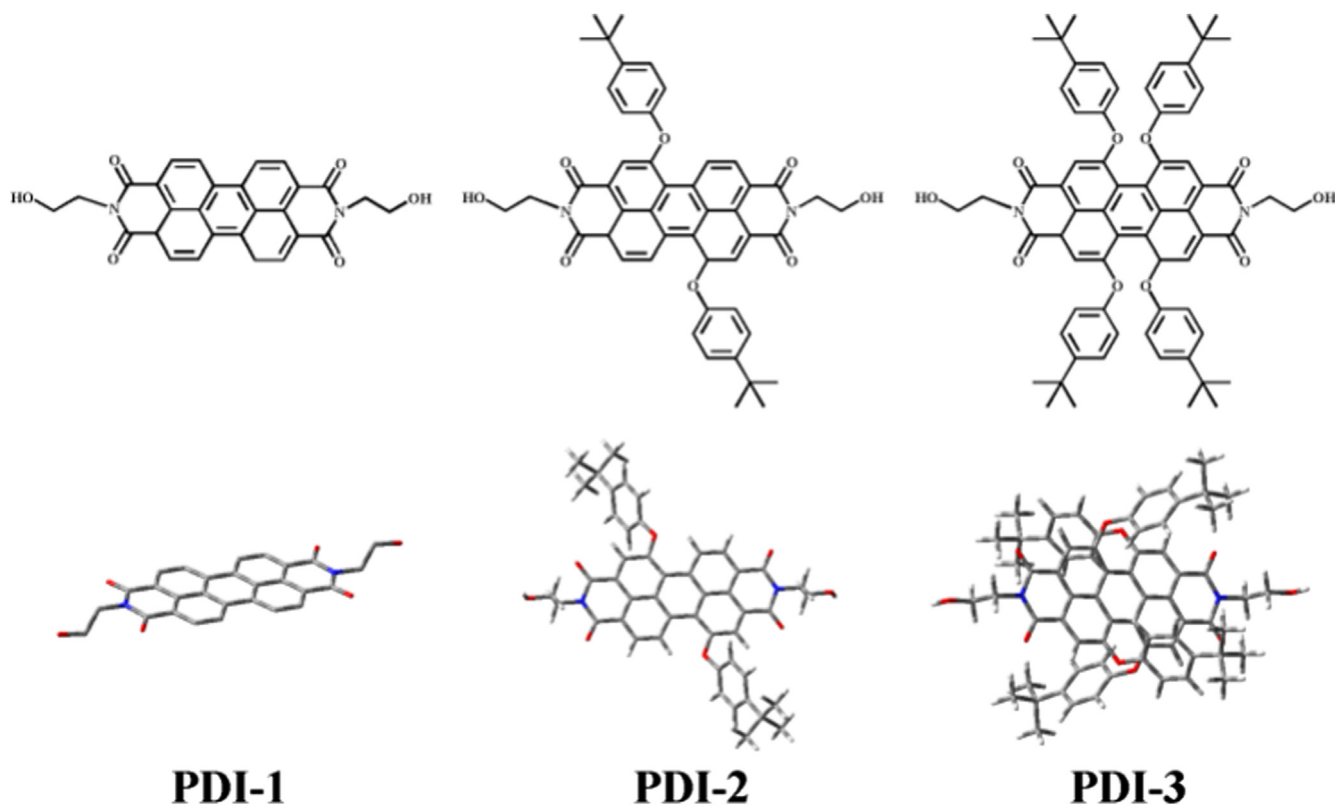
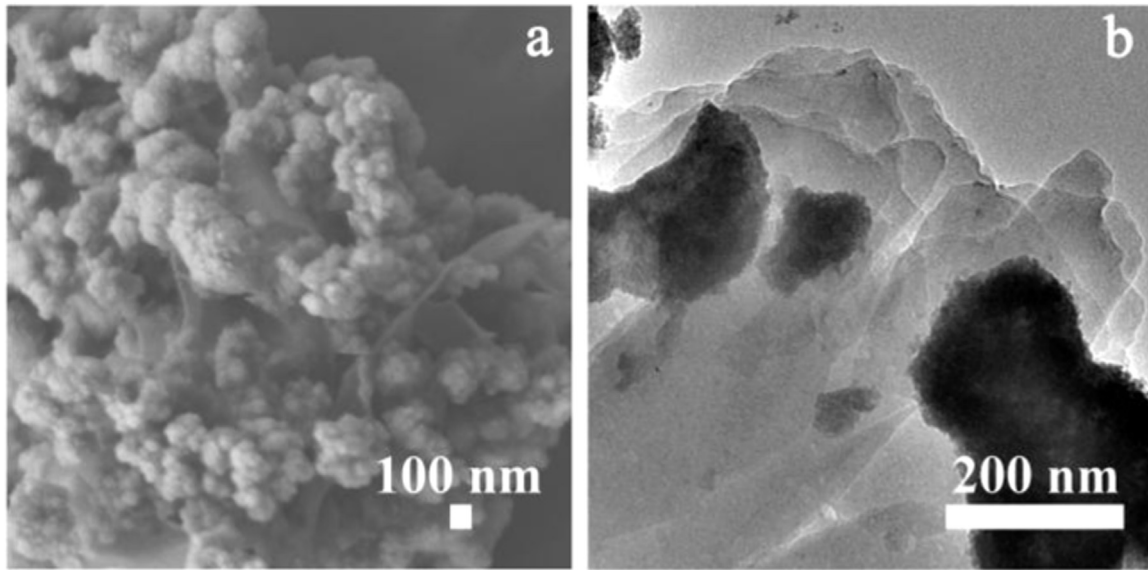**Scheme 1.** Molecular structure and geometry-optimized structures of **PDIs 1 − 3**.

Fig. 1. (a) SEM and (b) HRTEM images of the **$Zn_{0.5}Cd_{0.5}S$-PDI-1** nanocomposite.

Compared with the loosely accumulated nanospheres of the pristine **$Zn_{0.5}Cd_{0.5}S$** (Fig. S2a and b), some membrane-like structure are observed upon loading **PDIs** as characterized by SEM and TEM (Figs. 1a and S2c–f), which may refer to the aggregated **PDIs**. Diffraction patterns of HR-TEM (Figs. 1b and S3) indicate the crystalline nature of **$Zn_{0.5}Cd_{0.5}S$** particles and the stacked membranes from the **PDIs**. These observations may suggest the heterojunction formation between the **$Zn_{0.5}Cd_{0.5}S$** and **PDIs** with occurrence of a compact and abundant interfacial contact.

Indexed from the X-ray diffraction, the crystal phase of the **$Zn_{0.5}Cd_{0.5}S$** solid solution is a hexagonal wurtzite CdS phase (Fig. S4) [33]. Negligible changes on the XRD patterns are observed upon loading **PDIs** onto the **$Zn_{0.5}Cd_{0.5}S$**, indicating that the lattice structure of **$Zn_{0.5}Cd_{0.5}S$** particles keeps unchanged in the presence of **PDIs**. As indicated by EDS measurements (Fig. S5 and Table S1) as well as the ICP results (Fig. S6), the composition of the Zn, Cd and S elements within the **$Zn_{0.5}Cd_{0.5}S$-PDIs** composites are virtually identical to that of the pristine **$Zn_{0.5}Cd_{0.5}S$**. Figs. S7 and S8 provide the XPS spectra of **$Zn_{0.5}Cd_{0.5}S$** and **$Zn_{0.5}Cd_{0.5}S$-PDIs**. Apparently, the coupled **PDIs** have no influence on the valence state of Zn and Cd, which are both kept in $+2$ states. A slight increase in the binding energy upon hybridization can be detected from Fig. S7, indicating the binding effect between Zn/Cd and **PDIs**, originated from the sorption capacity of **PDIs** on the surface of **$Zn_{0.5}Cd_{0.5}S$** solid solution [34].

FT-IR and Raman Scattering measurements were carried out to reveal the connection between **$Zn_{0.5}Cd_{0.5}S$** and **PDIs** in **$Zn_{0.5}Cd_{0.5}S$-PDIs** nanocomposite. The IR spectra of **$Zn_{0.5}Cd_{0.5}S$**, **PDIs** and **$Zn_{0.5}Cd_{0.5}S$-PDIs** are given in Fig. S9. Remarkably, the bending vibration of O-H at 1249–1290 cm^{-1} observed in **PDIs** shifted to 1256–1273 cm^{-1} in **$Zn_{0.5}Cd_{0.5}S$-PDIs** [35], which may indicative of the binding between **PDIs** and the **$Zn_{0.5}Cd_{0.5}S$** [36]. Besides, the stretching vibration of C=C on **PDIs** at 1588 cm^{-1} shifted to 1600 cm^{-1} in **$Zn_{0.5}Cd_{0.5}S$-PDIs** nanocomposite [37], as a result of the close packing of the **PDIs**, which is in line with the observed membrane structure within the composites. Aggregation induced peak displacement could also be observed from the Raman scattering as shown in Fig. S10. All the **PDIs** are oriented in flat on adsorption geometry onto the surface of **$Zn_{0.5}Cd_{0.5}S$** nanoparticles. For **$Zn_{0.5}Cd_{0.5}S$-PDI-1** and **$Zn_{0.5}Cd_{0.5}S$-PDI-2**, C−H bending and perylene ring stretching at 1292, 1366 cm^{-1}, respectively [38,39], and C=C stretching at 1567 and 1587 cm^{-1} shifted toward high
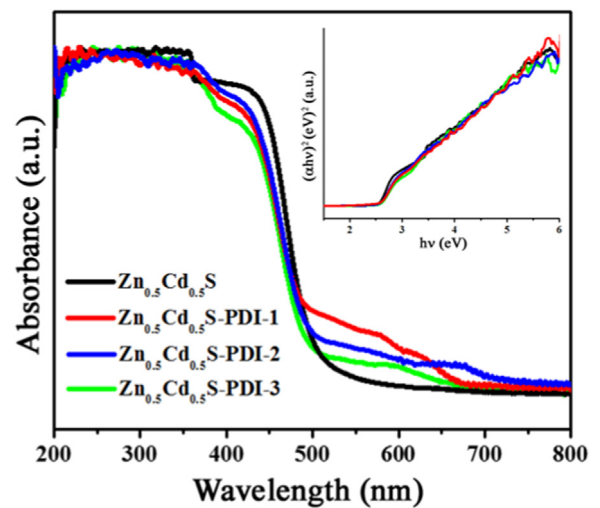

Fig. 2. UV–vis diffuse reflection spectra and band-gap calculation (inset) of **$Zn_{0.5}Cd_{0.5}S$**, **$Zn_{0.5}Cd_{0.5}S$-PDI-1**, **$Zn_{0.5}Cd_{0.5}S$-PDI-2** and **$Zn_{0.5}Cd_{0.5}S$-PDI-3**.
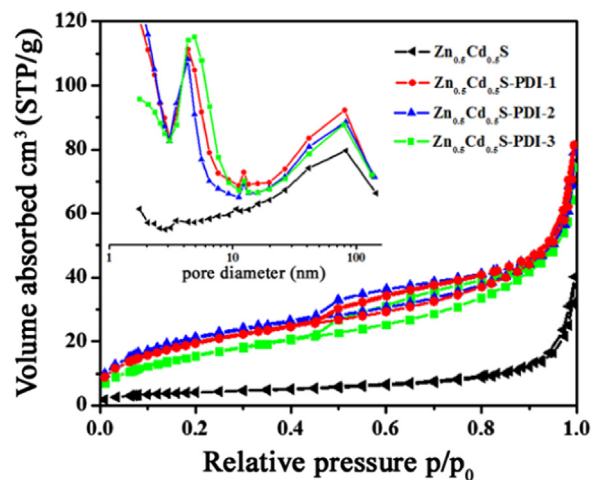

Fig. 3. Nitrogen adsorption-desorption isotherms and the corresponding pore size distribution curves (inset) of the **$Zn_{0.5}Cd_{0.5}S$**, **$Zn_{0.5}Cd_{0.5}S$-PDI-1**, **$Zn_{0.5}Cd_{0.5}S$-PDI-2** and **$Zn_{0.5}Cd_{0.5}S$-PDI-3**.
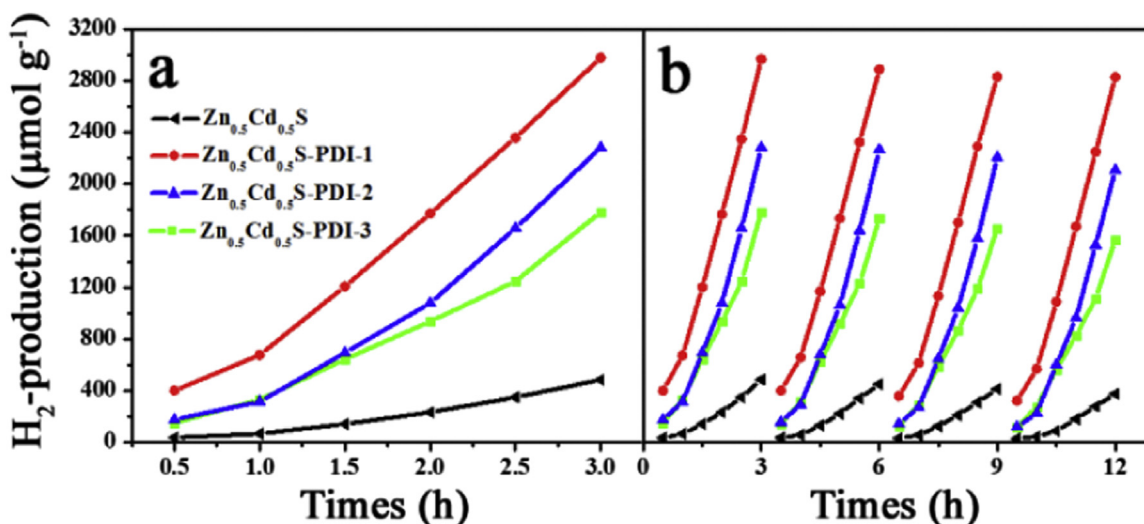
Fig. 4. Photocatalytic H_2-production activity under simulated solar irradiation over $Zn_{0.5}Cd_{0.5}S$, $Zn_{0.5}Cd_{0.5}S$-PDI-1, $Zn_{0.5}Cd_{0.5}S$-PDI-2, and $Zn_{0.5}Cd_{0.5}S$-PDI-3 samples.

frequency region relative to those of the scatterings in the corresponding **PDIs** molecules [39], **PDI-1** and **PDI-2**. However, no apparent peak-shift was observed for $Zn_{0.5}Cd_{0.5}S$-**PDI-3**, suggesting the loosely aggregated **PDI-3** within the composites, due to the largely twisted structure of the **PDI-3** as displayed in Scheme 1.

Fig. 2 depicts the UV – visible diffuse absorption spectra of $Zn_{0.5}Cd_{0.5}S$ and all the three $Zn_{0.5}Cd_{0.5}S$-**PDI** composites. Upon hybridization with **PDIs**, a weak but apparent broad absorption emerged in the visible region (from 500 to 700 nm), typically referring to the absorption from the **PDIs** with diverse molecular structure. The corresponding colour of the nanocomposite samples changes from yellow to dark yellow as can be distinguished by naked eyes (Fig. S11). Compared with their molecularly dispersed absorption in solution (Fig. S12), this broaden absorption clearly reveal the π-stacking offset between neighbouring perylene molecules, which is favouring for a lower-energy intermolecular charge transfer transition [40]. Specifically, as deduced from this absorption, **PDI-1** and **PDI-2** with more flat geometry of the aromatic core pack more densely than **PDI-3**, which is identified with the results revealed from Raman scattering.

According to the Kubelka-Munk method [41,42], the energy gap (E_g) of $Zn_{0.5}Cd_{0.5}S$ and $Zn_{0.5}Cd_{0.5}S$-**PDIs** can be estimated from the plots of $(\alpha h\nu)^2$ versus photon energy ($h\nu$), as shown in Fig. 2. The calculated E_g of the three $Zn_{0.5}Cd_{0.5}S$-**PDIs** are almost identical (2.28 eV) and quite equal to that of $Zn_{0.5}Cd_{0.5}S$ (2.36 eV), implying **PDI** is not incorporated into the lattice of $Zn_{0.5}Cd_{0.5}S$.

Fig. 3 demonstrates the nitrogen adsorption–desorption isotherms and the corresponding pore size distribution curves of the $Zn_{0.5}Cd_{0.5}S$ and the $Zn_{0.5}Cd_{0.5}S$-PDIs nanocomposites. Overall, the introduction of PDIs gives rise to increased Brunauer – Emmett – Teller (BET) surface areas of the composites relative to that of the pure $Zn_{0.5}Cd_{0.5}S$. Specifically, the BET surface area increases from 15.14 $m^2 g^{-1}$ of $Zn_{0.5}Cd_{0.5}S$ to 78.23 $m^2 g^{-1}$ of $Zn_{0.5}Cd_{0.5}S$-PDI-2 (Table S2).

Generally, photocatalysts with higher specific surface area are beneficial for the enhancement of photocatalytic performance [43]. Such an increased surface area can supply more surface active sites, make charge-carrier transport easier, and lead to enhanced photocatalytic performance. The increased surface area contributed mainly from the stacked membranes formed from the aggregation of **PDIs** (HRTEM observation in Fig. 1b), which forms large amount of mesopores (type IV of the nitrogen adsorption – desorption isotherms) as evidenced by the emerged

peak at around 4.32 nm in Fig. 3. It is worthy to note that delicate distinction on BET surface area and the pore distribution can be observed between the different **PDI**-containing composites, which may rise from the discrepancy of the molecular structures. Indeed, **PDIs** with different bay-substitution are inclined to stack in different manner [44]. The geometry-optimized structures (Scheme 1) illustrate how the increasing bulk of the bay-substituents sterically encumber π-stacking.

2.2. Photocatalytic H_2 production from water

Photocatalytic H_2-production activities of the as-prepared $Zn_{0.5}Cd_{0.5}S$-**PDIs** composites were evaluated under simulated solar irradiation (AM1.5, 100 mW/cm [2]) from an aqueous solution containing Na_2S and Na_2SO_3 as the sacrificial reagent. As shown in Fig. 4, $Zn_{0.5}Cd_{0.5}S$ demonstrates a relatively low photocatalytic activity, which is ascribed to the rapid recombination of photogenerated electrons and holes [32,45] combined with the low surface area aforementioned. Upon doping the **PDIs**, the overall photocatalytic activities enhanced remarkably from 4 to 6 folds. H_2 is produced rather linearly with irradiation time with the following order of activity: $Zn_{0.5}Cd_{0.5}S$-**PDI-1** > $Zn_{0.5}Cd_{0.5}S$-**PDI-2** > $Zn_{0.5}Cd_{0.5}S$-**PDI-3** > $Zn_{0.5}Cd_{0.5}S$. The highest rate of 1.32 mmol $h^{-1} g^{-1}$ is achieved on a $Zn_{0.5}Cd_{0.5}S$-**PDI-1** composite photocatalyst, which is comparable to the results of the reduced graphene oxide (RGO)-$Zn_xCd_{1-x}S$ nanocomposite [46]. Notably, it was clarified that such high H_2-evlution rate of (RGO)-$Zn_xCd_{1-x}S$ nanocomposite made RGO a new cocatalyst for replacing noble metals. Accordingly, herein we deduced that small organic π-conjugated molecules like **PDIs** may also act as promising cocatalyst, whose structure can be well tailored facilely. Fig. 4b shows the reaction time courses of H_2-production over $Zn_{0.5}Cd_{0.5}S$, $Zn_{0.5}Cd_{0.5}S$-**PDI-1**, $Zn_{0.5}Cd_{0.5}S$-**PDI-2**, $Zn_{0.5}Cd_{0.5}S$-**PDI-3** under visible light irradiation ($\lambda \geq 420$ nm). After four recycles, the photocatalytic H_2-production rate of $Zn_{0.5}Cd_{0.5}S$-**PDIs** decreased a little, indicating the good stability for hydrogen generation. It should be noted that no hydrogen was detected when **PDI** alone was used as a photocatalyst, suggesting that the bare **PDI** is unlikely active for photocatalytic H_2 production under our experimental conditions. In addition, control experiments indicate that no appreciable hydrogen production was detected in the absence of either irradiation or photocatalyst, suggesting that hydrogen was produced by photocatalytic reaction.
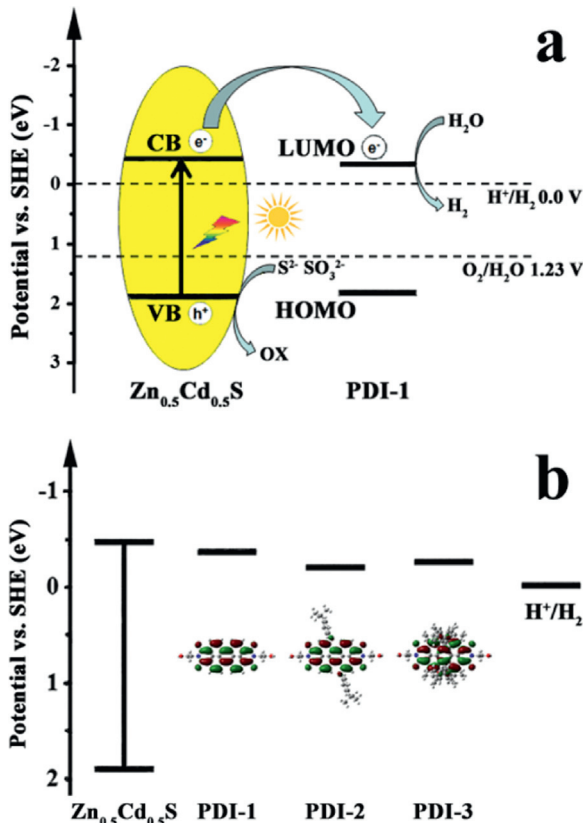
Scheme 2. Schematic illustration of the photocatalytic performance of the $Zn_{0.5}Cd_{0.5}S$-PDIs with (a) proposed mechanism for photocatalytic H_2-production under simulated solar irradiation and (b) the energy level diagram of $Zn_{0.5}Cd_{0.5}S$, **PDI-1**, **PDI-2**, and **PDI-3**.

2.3. Mechanisms accounting for the enhanced visible-light photocatalytic activity of $Zn_{0.5}Cd_{0.5}S$-PDIs nanocomposites

According to the above results, the markedly enhanced H_2-production activities of the $Zn_{0.5}Cd_{0.5}S$-PDIs nanocomposites should rely on two main factors: first, the increased surface area at the presence of mesopores formed from the aggregated **PDIs**; second, long-lived charge separated states manipulated by **PDIs**. Since all of the three **PDI** decorated nanocomposites demonstrate enhanced H_2-evlution rate with enhanced surface area relative to that of the pristine $Zn_{0.5}Cd_{0.5}S$, it is safely to conclude that the

increased surface area deduced from the aggregated **PDIs** contributed a lot to the H_2-evlution rate promotion, which is in line with previous reports [47]. However, special attention should be paid that compared with the three nanocomposite with different **PDIs**, the H_2-evlution rate promotion is not direct proportion to the surface area enhancement. It should therefore consider the key role of the **PDIs** in intervention the steps of the water splitting reaction.

For bare $Zn_xCd_{1-x}S$ solid solutions, under solar irradiation, electrons are excited from the valence band (VB) populated by S 3p to the formed CB by hybridizing Zn 4s4p with Cd 5s5p [15], and creates holes in VB. Generally, these charge carriers recombine rapidly before reaching the surface to reduce the H^+. It suggests that **PDI** can separate and store the photogenerated electrons, consequently reducing the recombination rate of the photogenerated electrons and holes therefore enhancing the activity of H_2-production. The interaction between the **PDIs** and the $Zn_{0.5}Cd_{0.5}S$ were checked with spectral analysis and electrochemical characterization.

The CB levels of $Zn_{0.5}Cd_{0.5}S$ (CB, -0.45 eV) were calculated according to approaches of Ginley and Frese reported in reference [48]. The energy levels of **PDIs** were estimated from the electronic absorption spectra (Fig. S12) and cyclic voltammetry (Table S4). The CB levels of $Zn_{0.5}Cd_{0.5}S$ is sufficiently negative relative to the LUMO of **PDIs**, the electron transfer from the CB of $Zn_{0.5}Cd_{0.5}S$ to the LUMO of **PDI** is therefore reasonable, which effectively enhances the separation of charge carriers and photocatalytic H_2 production performance. The charge transfer and separation in the $Zn_{0.5}Cd_{0.5}S$-PDI system is illustrated in Scheme 2.

Steady-state fluorescence spectra provide solid evidence for the above suggested electron communication process. According to the electronic absorption spectra of the $Zn_{0.5}Cd_{0.5}S$ and **PDIs** (Figs. 2 and S12), the $Zn_{0.5}Cd_{0.5}S$ and **PDIs** within the $Zn_{0.5}Cd_{0.5}S$-PDIs composites can be excited respectively. Upon excitation of the $Zn_{0.5}Cd_{0.5}S$ components with 465 nm light, where $Zn_{0.5}Cd_{0.5}S$ and **PDIs** were both excited, fluorescence from **PDIs** was severely quenched as shown in Fig. S13. Quantum yield and lifetime were too low to be detected. While selectively excite the **PDIs** within $Zn_{0.5}Cd_{0.5}S$-PDIs with 515 nm, where $Zn_{0.5}Cd_{0.5}S$ remains unexcited, strong emission from **PDIs** were observed, indicating no electron transition occurred from the excited **PDIs** to $Zn_{0.5}Cd_{0.5}S$ (Fig. S14). Overall, the above results demonstrate that the presence of **PDIs** function as an electron collector and transporter, which is significant to lengthen the lifetime of the charge carriers, consequently improve the charge separation and photocatalytic activity.

The light-absorption capability and the efficiency of electron
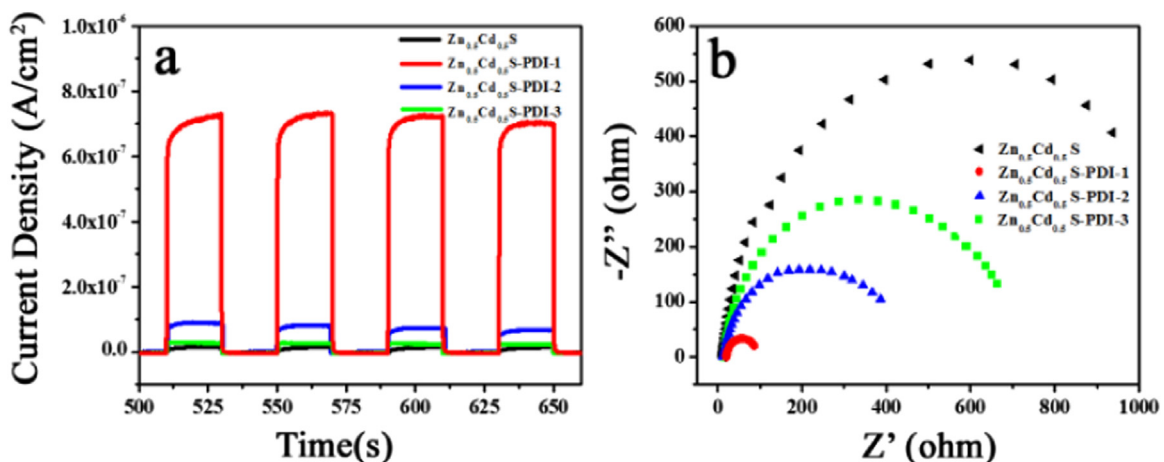
Fig. 5. (a) Transient photocurrent responses and (b) Nyquist plots of $Zn_{0.5}Cd_{0.5}S$, $Zn_{0.5}Cd_{0.5}S$-PDI-1, $Zn_{0.5}Cd_{0.5}S$-PDI-2, and $Zn_{0.5}Cd_{0.5}S$-PDI-3 electrodes in 0.5 M Na_2SO_4 solution under solar irradiation.

transfer from the CB edge position of the $Zn_{0.5}Cd_{0.5}S$ solid solutions to LUMO of **PDIs** rely on the energy matching and electron tunnelling between the neighbouring molecules, concerning the electron-withdrawing nature of the **PDIs**, which depends on the substitution effects on the **PDIs**. Consequently, three **PDIs** with different number of butyl-phenoxyl groups substituted at the bay-position of **PDI** framework are studied to disclose the above issue. The energy levels of three **PDIs** together with that of $Zn_{0.5}Cd_{0.5}S$ are depicted in Scheme 2b based on the spectroscopic data and cyclic voltammetry results (Fig. S12, Table S3). In general, CB of $Zn_{0.5}Cd_{0.5}S$ is more negative than the LUMO levels of all the **PDIs**, suggesting the electron transition from the CB of $Zn_{0.5}Cd_{0.5}S$ are allowed for all the three **PDIs**. Compared with **PDI-1**, **PDI-2** and **PDI-3** bare more positive LUMO levels, which is contradictory to the calculated results from the molecular simulation (Fig. S15). Indeed, substitution of **PDI** with electron-donating butyl-phenoxyl groups will cause decreased electron-withdrawing capability of the **PDIs** with negatively shifted LUMOs. The discrepancy between the experimental and calculated results should stem from the more inclined aggregation behaviour of **PDI-1** that has flat molecular structure [49]. On account the molecule aggregation (as also observed by SEM in Fig. S2c and e), LUMO level of **PDI-1** shifted negatively and well matched with the CB of the $Zn_{0.5}Cd_{0.5}S$ as shown in Scheme 2b, which is in favour of electron collection and transportation, resulting in the highest H₂-production rate of the $Zn_{0.5}Cd_{0.5}S$-PDI-1 as demonstrated in Fig. 4. On the other hand, although the LUMO level of $Zn_{0.5}Cd_{0.5}S$-PDI-3 is more negative than that of $Zn_{0.5}Cd_{0.5}S$-PDI-2, $Zn_{0.5}Cd_{0.5}S$-PDI-3 shows the lowest H₂-production efficiency. This is reasonable since by four large butyl-phenoxyl groups substitution, other than the weakened electron-accepting ability, **PDI-3** has a highly twisted molecular structure, which is against the electron transfer between the **PDI** molecules, therefore cannot prevent the electron-hole recombination effectively. Overall, taking both structure and photoelectric properties, **PDI-1** is the most ideal material of doping. More interestingly, the above results imply that electron transition between the $Zn_{0.5}Cd_{0.5}S$ and the **PDIs** can be elaborately manipulated by subtle molecular design and tailor.

To provide an additional evidence for the above suggested photocatalytic mechanism, the transient photocurrent responses of $Zn_{0.5}Cd_{0.5}S$ and the $Zn_{0.5}Cd_{0.5}S$-PDIs were recorded for several on–off cycles of solar irradiation. Fig. 5a shows a comparison of the photocurrent–time (I–t) curves with typical on–off cycles of intermittent solar irradiation without bias potential. An apparently boosted photocurrent response appears for all the samples under solar illumination, and the on–off cycles of the photocurrent are reproducible. This indicates that most of photo-generated electrons are transported to the back contact across the sample to produce photocurrent under solar irradiation [50]. Notably, all the **PDI** doped samples showed promoted transient photocurrent compared with the pristine $Zn_{0.5}Cd_{0.5}S$. The transient photocurrent shows a relatively slow response without anodic photocurrent spikes when the light is switched on and off for the $Zn_{0.5}Cd_{0.5}S$-PDIs. It was reported that by incorporation of an electron-captor with lower Fermi level than that of the CB electrons, electrons can be trapped by the electron-captor, resulting in slow photocurrent responses [51]. Here, **PDI** serves as an electron collector and the photoelectrons were trapped by **PDIs**, which slowdown the transportation of the electrons to the back contact electrode upon illumination. When switching off the irradiation, charge carriers release from the traps to form the slow response of the photocurrent decaying to zero [51]. In short, the **PDI** can separate and store photo-generated electrons, therefore effectively restrain the charge recombination, leaving more charge carriers to form reactive species, which in turn results in the high photocurrent response and photocatalytic H₂-production rate.

As expected, the highest transient photocurrent was obtained for $Zn_{0.5}Cd_{0.5}S$-PDI-1, which is more than 6 time higher than that of the pristine $Zn_{0.5}Cd_{0.5}S$, and much higher than $Zn_{0.5}Cd_{0.5}S$-PDI-2 and $Zn_{0.5}Cd_{0.5}S$-PDI-3. Considering the above photo-activated H₂-evolution results (Fig. 4), the highest H₂-production activity of $Zn_{0.5}Cd_{0.5}S$-PDI-1 is mainly determined by suppressed charge recombination with participation of **PDI-1**, rather than the improved specific surface area. As clarified above, molecular structure has great effect on the **PDIs** function as the electron acceptor and transporter, concerning the energy level matching and electron transporting efficiency. The electron donating substituents of butyl-phenoxyls at bay position affect the electron-accepting ability and the π-stacking of **PDIs**. Generally, parallel stacking is favoured for charge carrier mobility due to the strong π-electron delocalization between the packed molecules [52,53]. Therefore, **PDI-1** with the strong electron-withdrawing ability, matched LUMO level (to CB of $Zn_{0.5}Cd_{0.5}S$), and the plane conformation is best for retarding the recombination of the photo-generated electrons and holes within the $Zn_{0.5}Cd_{0.5}S$-PDIs composites.

Electrochemical impedance spectroscopy (EIS) Nyquist plots were recorded to study the charge-transfer process occurring between the catalyst and electrode surface. Fig. 5b shows the EIS Nyquist plots of all the samples measured at a bias potential of 0.5 V. The $Zn_{0.5}Cd_{0.5}S$-PDI-1 shows the smallest semicircle in the middle-frequency region in comparison to the pristine $Zn_{0.5}Cd_{0.5}S$, $Zn_{0.5}Cd_{0.5}S$-PDI-2 and $Zn_{0.5}Cd_{0.5}S$-PDI-3, indicating the fastest interfacial electron transfer. Overall, on account of the excellent conductivity, the introduction of **PDI** can benefit the charge transfer in the $Zn_{0.5}Cd_{0.5}S$-PDIs and thus lower the charge recombination. Among the three **PDIs**, **PDI-1** has the strongest ability of electron transfer. In short, **PDI** can function as an electron collector in the composite to inhibit the charge recombination, which is crucial for optimizing the photocatalytic activity of $Zn_{0.5}Cd_{0.5}S$-PDIs nanocomposites. The photo-induced electrons transfer onto the PDIs, make them newly generated sites for water splitting [46,54]. The closely stacked membrane-like structure formed from PDIs aggregation provide platform for electron collection and transmission, greatly enhancing the H₂ production. Moreover, in this work, we present for the first time that the charge transfer efficiency between the $Zn_{0.5}Cd_{0.5}S$ semiconductor and the **PDIs** electron acceptor can be fine-tuned by tailoring the molecular structure of **PDIs**, which has significant effect on the charge recombination.

3. Conclusions

In summary, the present work provides a new insight for design and development of organic molecule modified photocatalysis. It is demonstrated that organic dyes with large π-conjugated structure may significantly enhanced hydrogen production performance by suppressing photoexcited charge carriers recombination through an electron transfer process. $Zn_{0.5}Cd_{0.5}S$ was bonded with electron collector **PDIs** *in situ* to form $Zn_{0.5}Cd_{0.5}S$-PDIs nanocomposites facilely, where photogenerated electrons on CB of $Zn_{0.5}Cd_{0.5}S$ transfer promptly to the LUMO of PDIs to realize the inhibition of the electron-hole recombination. The charge transition and the H₂-production rate depend heavily on the molecular structure of the decorated **PDIs**, concerning mainly the energy level matching between $Zn_{0.5}Cd_{0.5}S$ and **PDIs**. For a **PDI-1** contained $Zn_{0.5}Cd_{0.5}S$-PDI-1 at a content of 0.5 wt%, a high H₂-evolution rate of 1.32 mmol h^{-1} g^{-1} is achieved, which is 6 folds of the pristine $Zn_{0.5}Cd_{0.5}S$ and much higher than that of $Zn_{0.5}Cd_{0.5}S$-PDI-2 and $Zn_{0.5}Cd_{0.5}S$-PDI-3. The correlation of the electron transition efficiency with the substitution effect on **PDIs** is therefore disclosed. Overall, the results demonstrate that the

unique features of **PDIs** make it an excellent electron collector and transporter for **Zn$_{0.5}$Cd$_{0.5}$S** nanoparticles, and the electron communication between them can be well manipulated by tailoring the PDIs molecular structure. Besides, **PDIs** are aggregated in the **Zn$_{0.5}$Cd$_{0.5}$S-PDIs** composites, providing a large number of mesopores to increase specific surface area and active sites for photocatalytic reactions. Substitution on the **PDIs** also has great effects on the aggregation behaviour of **PDIs**, which will significantly intervene with the charge separation and recombination within the system. This issue will be investigated in detail in our future work.

Acknowledgements

Appendix A. Supplementary material

Supplementary data associated with this article can be found in the online version at http://dx.doi.org/10.1016/j.nanoen.2016.04.058.

References

[1] A. Fujishima, Nature 238 (1972) 37–38.
[2] A. Kudo, Y. Miseki, Chem. Soc. Rev. 38 (2009) 253–278.
[3] C. Xing, Y. Zhang, W. Yan, L. Guo, Int. J. Hydrog. Energy 31 (2006) 2018–2024.
[4] W. Li, D. Li, Z. Chen, H. Huang, M. Sun, Y. He, X. Fu, J. Phys. Chem. C. 112 (2008) 14943–14947.
[5] J.S. Hu, L.L. Ren, Y.G. Guo, H.P. Liang, A.M. Cao, L.J. Wan, C.L. Bai, Angew. Chem. 117 (2005) 1295–1299.
[6] J. Shi, H.n. Cui, Z. Liang, X. Lu, Y. Tong, C. Su, H. Liu, Energy Environ. Sci. 4 (2011) 466–470.
[7] M. Liu, L. Wang, G.M. Lu, X. Yao, L. Guo, Energy Environ. Sci. 4 (2011) 1372–1378.
[8] J. Villoria, R.M. Navarro Yerga, S. Al-Zahrani, J.L.G. Fierro, Ind. Eng. Chem. Res. 49 (2010) 6854–6861.
[9] K. Zhang, D. Jing, Q. Chen, L. Guo, Int. J. Hydrog. Energy 35 (2010) 2048–2057.
[10] W. Zhang, R. Xu, Int. J. Hydrog. Energy 34 (2009) 8495–8503.
[11] M. Nguyen, P.D. Tran, S.S. Pramana, R.L. Lee, S.K. Batabyal, N. Mathews, L. H. Wong, M. Graetzel, Nanoscale 5 (2013) 1479–1482.
[12] W. Li, D. Li, S. Meng, W. Chen, X. Fu, Y. Shao, Environ. Sci. Technol. 45 (2011) 2987–2993.
[13] S. Xie, X. Lu, T. Zhai, J. Gan, W. Li, M. Xu, M. Yu, Y.-M. Zhang, Y. Tong, Langmuir 28 (2012) 10558–10564.
[14] H. Wu, Y. Yao, W. Li, L. Zhu, N. Ni, X. Zhang, J. Nanopart. Res. 13 (2011) 2225–2234.
[15] L. Wang, Z. Yao, F. Jia, B. Chen, Z. Jiang, Dalton Trans. 42 (2013) 9976–9981.
[16] W. Xu, X. Meng, W. Ji, P. Jing, J. Zheng, X. Liu, J. Zhao, H. Li, Chem. Phys. Lett. 532 (2012) 72–76.
[17] J. Zhang, Q. Xu, S.Z. Qiao, J. Yu, ChemSusChem 6 (2013) 2009–2015.
[18] Y. Zhao, M.R. Wasielewski, Tetrahedron Lett. 40 (1999) 7047–7050.
[19] J.M. Serin, D.W. Brousmiche, J.M. Fréchet, J. Am. Chem. Soc. 124 (2002) 11848–11849.
[20] Z. Chen, M.G. Debije, T. Debaerdemaeker, P. Osswald, F. Würthner, ChemPhysChem 5 (2004) 137–140.
[21] C.-C. Chao, M.-k. Leung, Y.O. Su, K.-Y. Chiu, T.-H. Lin, S.-J. Shieh, S.-C. Lin, J. Org. Chem. 70 (2005) 4323–4331.
[22] P. Osswald, D. Leusser, D. Stalke, F. Würthner, Angew. Chem. Int. Ed. 44 (2005) 250–253.
[23] H. Qian, C. Liu, Z. Wang, D. Zhu, Chem. Commun. (2006) 4587–4589.
[24] F. Würthner, P. Osswald, R. Schmidt, T.E. Kaiser, H. Mansikkamäki, M. Könemann, Org. Lett. 8 (2006) 3765–3768.
[25] Y. Li, L. Tan, Z. Wang, H. Qian, Y. Shi, W. Hu, Org. Lett. 10 (2008) 529–532.
[26] T. Abe, K. Nagai, S. Kabutomori, M. Kaneko, A. Tajiri, T. Norimatsu, Angew. Chem. Int. Ed. 45 (2006) 2778–2781.
[27] J.T. Kirner, J.J. Stracke, B.A. Gregg, R.G. Finke, ACS Appl. Mater. Interfaces 6 (2014) 13367–13377.
[28] S. Chen, D.L. Jacobs, J. Xu, Y. Li, C. Wang, L. Zang, RSC Adv. 4 (2014) 48486–48491.
[29] F. Ronconi, Z. Syrgiannis, A. Bonasera, M. Prato, R. Argazzi, S. Caramori, V. Cristino, C.A. Bignozzi, J. Am. Chem. Soc. 137 (2015) 4630–4633.
[30] J. Song, Q. Tian, J. Gao, H. Wu, Y. Chen, X. Li, CrystEngComm 16 (2014) 1277–1286.
[31] Q. Li, H. Meng, P. Zhou, Y. Zheng, J. Wang, J. Yu, J. Gong, ACS Catal. 3 (2013) 882–889.
[32] J. Zhang, L. Qi, J. Ran, J. Yu, S.Z. Qiao, Adv. Energy Mater. 4 (2014).
[33] A.B. Suganthi, P. Sagayaraj, Mater. Chem. Phys. 139 (2013) 917–922.
[34] T. Nonoyama, T. Kinoshita, M. Higuchi, K. Nagata, M. Tanaka, K. Sato, K. Kato, J. Am. Chem. Soc. 134 (2012) 8841–8847.
[35] S. Corrêa, L.C.T. Lacerda, M. Pires, J. Nanomater. 2015 (2016) 1–7.
[36] X. Wei, R. Zhao, M. Shao, Nano Res. Lett. 8 (2013) 112.
[37] Y. Wu, B. Li, W. Wang, Mater. Sci. Eng. C 23 (2003) 605–609.
[38] D.A. Tenne, S. Park, T.U. Kampen, A. Das, Phys. Rev. B 61 (2000) 14564–14569.
[39] K. Akers, R. Areca, J. Phys. Chem. 91 (1987) 2954–2959.
[40] J.J. Han, W. Wang, A.D. Li, J. Am. Chem. Soc. 128 (2006) 672–673.
[41] J. Ng, S. Xu, X. Zhang, H.Y. Yang, D.D. Sun, Adv. Funct. Mater. 20 (2010) 4287–4294.
[42] N. Serpone, D. Lawless, R. Khairutdinov, J. Phys. Chem. 99 (1995) 16646–16654.
[43] K.-I. Ishibashi, A. Fujishima, T. Watanabe, K. Hashimoto, Electrochem. Commun. 2 (2000) 207–210.
[44] R. Schmidt, M.M. Ling, J.H. Oh, M. Winkler, M. Könemann, Z. Bao, F. Würthner, Adv. Mater. 19 (2007) 3692–3695.
[45] Q. Li, H. Meng, J. Yu, W. Xiao, Y. Zheng, J. Wang, Chem. – A Eur. J. 20 (2014) 1176–1185.
[46] J. Zhang, J. Yu, M. Jaroniec, J.R. Gong, Nano Lett. 12 (2012) 4584–4589.
[47] Q. Xiang, J. Yu, M. Jaroniec, J. Am. Chem. Soc. 134 (2012) 6575–6578.
[48] S.R. Morrison, OSTI, 1980.
[49] M. Adachi, Y. Nagao, Chem. Mater. 13 (2001) 662–669.
[50] A. Hagfeldt, H. Lindström, S. Södergren, S.-E. Lindquist, J. Electroanal. Chem. 381 (1995) 39–46.
[51] J. Yu, G. Dai, B. Huang, J. Phys. Chem. C 113 (2009) 16394–16401.
[52] X. Crispin, J. Cornil, R. Friedlein, K.K. Okudaira, V. Lemaur, A. Crispin, G. Kestemont, M. Lehmann, M. Fahlman, R. Lazzaroni, J. Am. Chem. Soc. 126 (2004) 11889–11899.
[53] A. Rochefort, R. Martel, P. Avouris, Nano Lett. 2 (2002) 877–880.
[54] J. Yu, B. Yang, B. Cheng, Nanoscale 4 (2012) 2670–2677.